



Radio Science

RESEARCH ARTICLE

10.1029/2019RS006920

Special Section:

Advances in Electromagnetics, Photonics, Signal Processing, and Communication Technology

Key Points:

- IoT network communications study for small HF antennas based on low power transmission
- Study of narrowband modulations variating its power transmission and bandwidth
- QAM is the best modulation for low-power transmission with NVIS system on Antarctica environment

Correspondence to:

J. L. Pijoan,
joanlluis.pijoan@salle.url.edu

Citation:

Porte, J., Maso, J. M., Pijoan, J. L., & Badia, D. (2020). Sensing system for remote areas in Antarctica. *Radio Science*, 55, e2019RS006920. <https://doi.org/10.1029/2019RS006920>

Received 9 JUL 2019

Accepted 2 FEB 2020

Accepted article online 5 FEB 2020

Sensing System for Remote Areas in Antarctica

Joaquim Porte¹ ID, Josep M. Maso¹, Joan Lluis Pijoan¹ ID, and David Badia¹

¹Research Group in Internet Technologies and Storage (GRITS), La Salle Ramon Llull, Barcelona, Spain

Abstract Every year, the number of Internet of Things devices is growing exponentially. The current Internet of Things technology to support the connectivity of such a huge number of devices is limited by the coverage of the base stations deployed. In case of remote areas without coverage of any operator, the use of a satellite connection is such a high-cost option. The only alternative option for very remote sensor is high frequency (HF) communications with ionospheric reflection. The HF band (3–30 MHz) with Near Vertical Incidence Skywave allows a large coverage area (up to 250 km) without the need of line of sight. The HF radio links usually need higher power transmissions with larger antennas supported by a mast. In this paper, we explore a new transmission scheme for low-power transmissions, which is equivalent to use small and low gain HF antennas. We study the performance of several digital modulations using different bandwidths and transmission power. The field tests have been done around the Spanish Antarctic Base at Livingston Island to ensure the availability of the system even in polar areas where the behavior of the ionosphere is quite different from lower latitudes. However, the proposed physical layer fits well with any other remote location that requires low power data communication.

1. Introduction

Every year, the number of Internet of Things (IoT) connected devices is increasing constantly. In 2019, the number of IoT devices are about 26.66 billion, and it is expected to increase exponentially up to 75.44 billion in 2025 Statista - Internet of Things - Number of connected devices worldwide 2015-2025, n.d.). Some radio technologies for communicating this exorbitant number of devices have emerged; however, the coverage areas (offered by Sigfox, Lora, Neul, etc) are quite limited (Lauridsen et al., 2017).

In case of remote sensors, which are far (more than 10 km) from the nearest base station, the only alternatives without line of sight are satellites and high frequency (HF) communications. Other solutions such as repetition of the signal following the orography will solve the problem. However, this solution has a high economic cost. The main drawbacks of satellite connections are the high costs of the service and the operator dependency. Moreover, the coverage area of satellites is limited at polar locations, since the geostationary satellites usually do not have line of sight, and it required a network of polar satellites.

As an alternative to the satellite connection, a radio link in the HF band (3–30 MHz; Davies, 1990) can be established. HF communications do not need line of sight between the transmitter and the receiver. The wave is reflected by the upper layers of the atmosphere, which are ionized by the ultraviolet radiation coming from the sun. Depending on the angle of incidence in the ionosphere, two types of communication can be achieved. In the case of long-distance communications (DX), the incidence angle is lower than 70°, and we can cover a distance of 3000 km per hop. In practice, we can communicate with any part of the world using four or five hops (Vilella et al., 2009). In the case of an incidence angle between 70° and 90°, we refer to Near Vertical Incidence Skywave (NVIS) communications, with only one reflection achieving a radio coverage up to 250 km (see Figure 1), assuming 350 km as the maximum height of the ionosphere, (Witvliet & Alsina-Pagès, 2017). In Figure 2, we can see a hypothetical scenario with the different radio technologies for remote IoT.

Antarctica is one of the most remote and isolated places in the world. Many research activities are developed in the scientific bases distributed throughout the continent among the year (AEMET, 2019). Most of the scientific studies are based on data collected from sensors. Some of them are far from the base, and the downloading of the data has to be made manually. In that context, the data transmission is only possible using satellite links or HF radio communications. The services of the most common satellite operators (Iridium, Inmarsat, Thuraya, etc) are usually expensive and need line of sight.

©2020. The Authors.

This is an open access article under the terms of the Creative Commons Attribution License, which permits use, distribution and reproduction in any medium, provided the original work is properly cited.

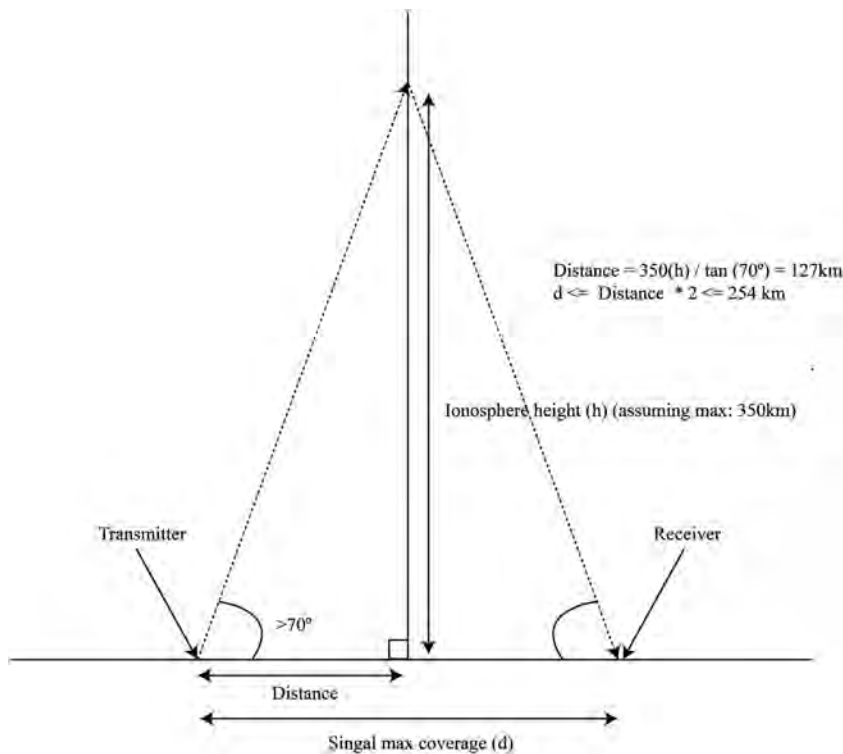


Figure 1. NVIS signal propagation coverage.

If we want to use HF communications for remote sensors, there are two key factors to be taken into account: First, the power consumption of the system, to increase the autonomy of the batteries and reduce the size as much as possible. Second, the size of the antenna, since we are dealing with wavelengths up to 100 m. For instance, a typical half-wave dipole at 4 MHz can reach 30 m and needs a mast of at least 12 m high. If a smaller antenna is installed, it will introduce some losses, which the receiver will have to handle with.

In this paper, we present a solution for a new physical layer for NVIS communications under two different hypotheses. First, in the case of limited transmission power (or lossy antennas) for battery powered systems, we find the best modulation scheme with a transmission power around 1 W. That will allow us to install small antennas, whenever the losses remain below 15 dB. Second, in the case of equipment connected to the mains, we try to maximize the bit rate using the best combination of modulation and bandwidth for a given transmission power.

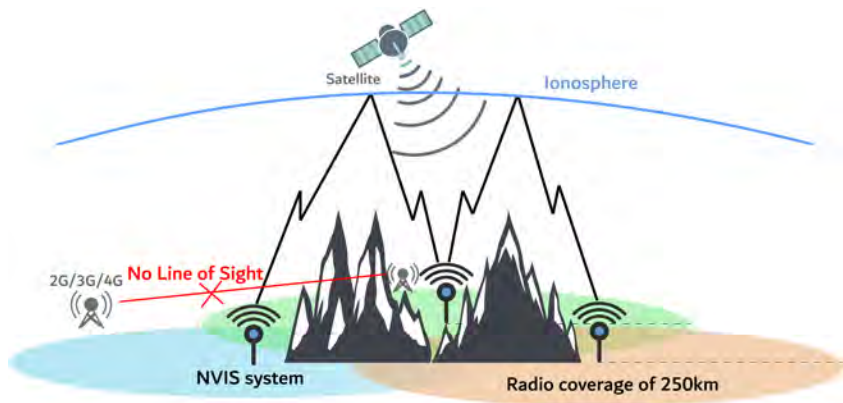


Figure 2. NVIS technology.



Figure 3. NVIS communications at Livingston Island.

The performance tests were carried out during the 2018–2019 Spanish Antarctic campaign in Livingston Island. We established an NVIS testbed from a remote location of the Spanish Antarctic Base Juan Carlos I. The remote node was placed at Rocky Glacier, 5.7 km away from the base. In Figures 3 and 4, we can see the node location and the elevation profile between the two nodes. The testbed was intended to study both the channel response and the physical layer in non-real-time mode, as well as the operation of the system in real-time.

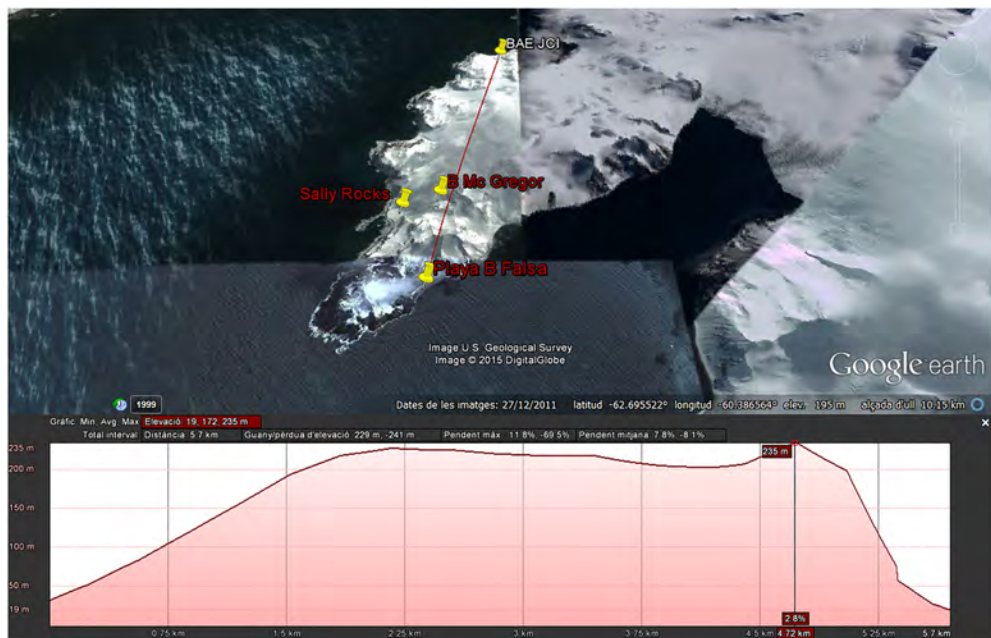


Figure 4. Elevation profile from the base to Rocky Glacier.

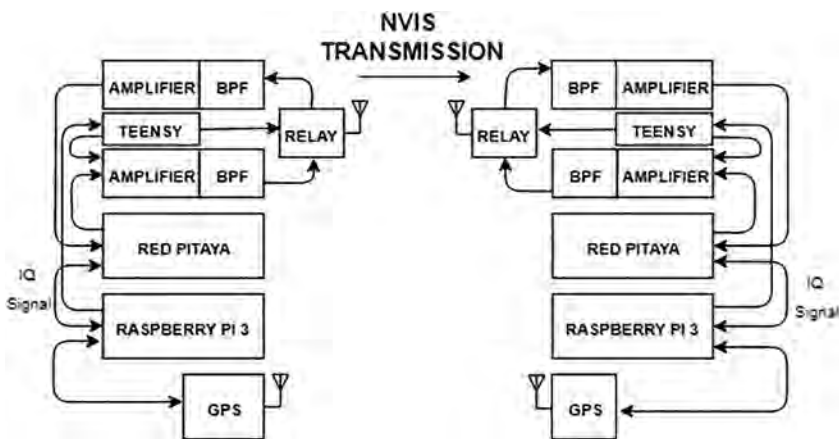


Figure 5. Schematic of the developed system.

This paper is organized as follows. In section 2, a description of the system is presented. In section 3, we detail the test bench and the frame distribution of every transmission. In section 4, the results obtained of the different tests are presented. Finally, section 6 contains the conclusions.

2. System Description

The main goal of the testbed is to test the influence of the transmission power, carrier frequency, hour of the day, bandwidth, and modulation scheme in the performance of an NVIS link. For that purpose, we need a complete reconfigurable software-defined radio platform.

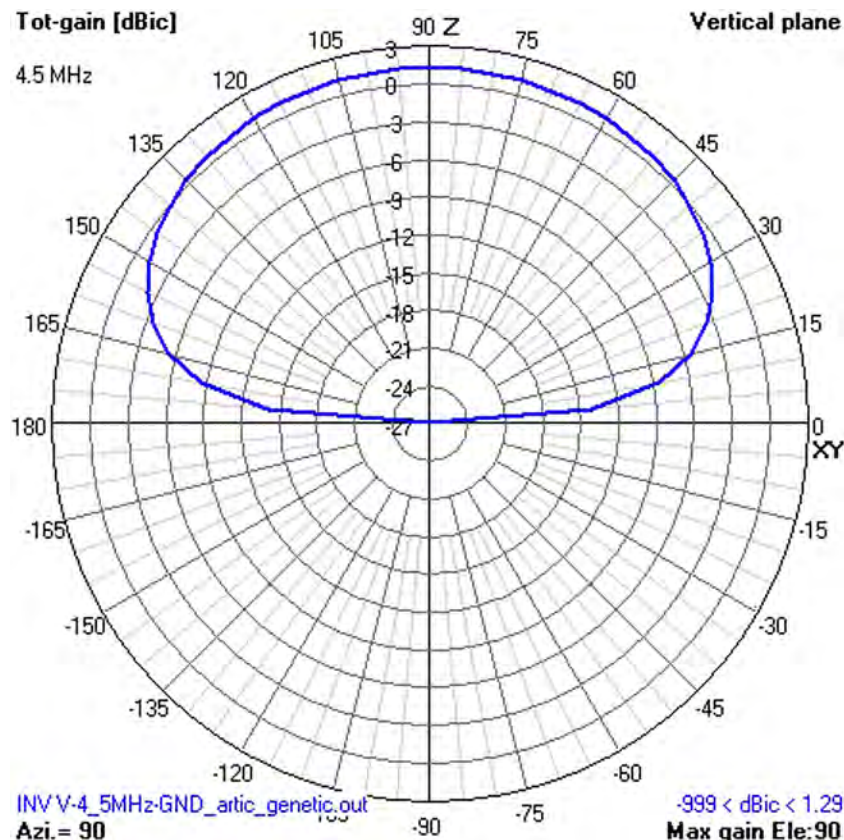


Figure 6. Radiation diagram of V-inverted at permafrost soil.

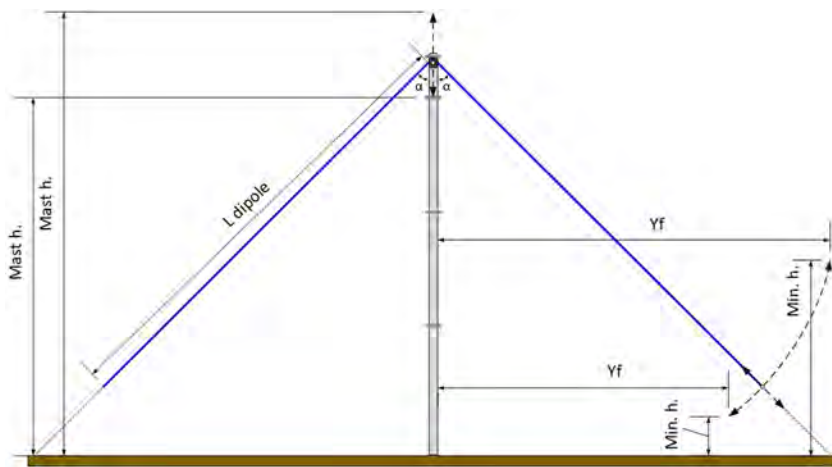


Figure 7. Dimensions of the inverted-V antenna.

2.1. Hardware Description

The hardware platform (see Figure 5) is based on available devices in the market, but all the programming code has been developed by our group in order to transmit and receive any kind of signal in both real-time and non-real-time (Porte, Maso, et al., 2019). It can also be programmed as a radio modem in real-time as we can see at Maso et al. (2019). Moreover, it allows optional GPS synchronization to help the timing adjust for the testing mode.

The hardware can be programmed to act as either a transmitter or a receiver. The system is composed principally by a Red Pitaya platform (Red Pitaya, n.d.) and a Raspberry Pi 3 together with some peripherals described below. The Red Pitaya platform is the core of the system, essentially composed by a Zynq 7010 chip. This chip is an Advanced RISC Machine (ARM) + Field-Programmable Gate Array (FPGA) and includes two analog to digital converters and two digital to analog converters. It is in charge in upsampling the baseband signals and downsampling the HF signal carrier (Kodali et al., 2013). A Linux operative system is running in the ARM, and it is programmed in C code, while the FPGA is programmed directly in VHDL code. This architecture allows the ARM and the FPGA to communicate in a very efficient way and to have a full control of all the parameters of the transmission.

On the other hand, the Raspberry Pi 3 is the microprocessor that interacts with the rest of the peripherals. This platform is also used with a Linux operative system and has been programmed in C code. It is connected to the Red Pitaya using an Ethernet connection and to the GPS, a Teensy module, and an external hard drive using a serial port. In reception mode, the Raspberry receives the HF signal after being downconverted to baseband and stores the IQ samples in the hard drive. In transmission mode, a crontab is set up to decide the hour and minute when every test frame has to be transmitted. In the right moment, the Raspberry sends the IQ frames via serial to the Red Pitaya and a message to the Teensy module. The Teensy is a microcontroller in charge of the control of the signal amplifier and the antenna relay. When it receives a message from Raspberry Pi 3 to go to TX mode, it switches on the amplifier and commutes the antenna relay to the power amplifier. The GPS module, endowed with an external GPS antenna, provides time-synchronization between transmitter and receiver for sounding proposes.

Table 1
Optimum Dimensions of the Inverted-V Antenna

Soil type	Optimization algorithm	Gain (dBi)	SWR	Impedance (Ω)	Mast h. (m)	Min h. (m)	Yf (m)
Ideal	Evolve	6.8	1.96	$25.6 + 3.2j$	11.01	2.00	12.39
Rural	Evolve	3.8	1.05	$47.7 + 0.4j$	10.81	1.87	12.39
Permafrost	Evolve	1.3	1.27	$63.3 - 1.0j$	13.08	2.00	11.51

Table 2
Power Transmission Tests

Order of modulation	Power transmission	Minute
2,4,8,16,32	1 W	05,06,07,08,09
2,4,8,16,32	3 W	15,16,17,18,19
2,4,8,16,32	6 W	25,26,27,28,29
2,4,8,16,32	12 W	35,36,37,38,39
2,4,8,16,32	24 W	45,46,47,48,49
2,4,8,16,32	6 W	55,56,57,58,59

Regarding the amplifiers, the system is composed by an Low Noise Amplifier for the receiving HF signal and a power amplifier for the transmitting HF signal from Red Pitaya. The maximum transmission power amplifier is limited to 250 W, but the tests have been done at much lower values.

2.2. Antenna

A small HF antenna will present negative gains from -5 to -10 dB. Instead of using such type of antenna, we will test our platform using a low power signal transmission, from 1 to 24 W, which values are very low compared to others HF transceivers of the market (“HF 3000|Thales Group, n.d.”; R&S®M3SR Series4100 Software Defined Radios\System Components|Rohde & Schwarz, n.d.), where the power transmission of these products is from 20 to 400 W.

For the modulation tests, we chose an inverted-V antenna as the best option as we can see in Porte, Pijoan, et al. (2019). This antenna is easy to install, as it only needs one central mast and has a gain of around 2 dB. As indicated above, in NVIS, the maximum of the radiation diagram of the antenna has to be between 70° and 90° to maximize the efficiency. In Figure 6, we can see how the simulation of an inverted-V over permafrost soil meets the specification.

As the size of the antenna is directly related to the wavelength, we have to decide first the transmission frequency. For vertical incidence, the optimum frequency is selected as 85% of the critical frequency of the F2 layer (foF2). The critical frequency is highly dependent on the season and the solar activity. After checking the historical records of the Ebre Observatory (Ionogrammes de Livingston, n.d.) and Lowell Digisonde International (LDI, Lowell Digisonde International Station List (Digisonde.com), n. d.), we found out an average foF2 of about 5.3 MHz, so a transmission frequency of 4.3 MHz was selected. The size of the antenna has been calculated as $L = c/4f$, resulting a branch length of 15.63 m. Other factors such as the mast height and the angle of aperture of the branches are key to achieve the optimum gain (see Figure 7). The height of the mast will configure the height of the antenna beyond the ground; this distance can create variations of the gain antenna because of reflections of the electromagnetic wave with the ground. By the other hand, the angle of aperture of the branches of the antenna also variates the antenna radiation diagram and the gain. These parameters have to be adjusted via simulation for a given type of soil (Witvliet et al., 2015). In Table 1, we can see the optimum values of the antenna dimensions for different types of soil.

The whole system (filters, matching networks) was optimized to operate at 4.3 MHz, which is the best frequency during the day. For night hours, the frequency should decrease, and a longer antenna should be used.

2.3. Amplifier

Although the linearity of the power amplifier is required for nonconstant envelope modulations, we wanted a linear amplifier to be able to test any kind of modulation. We installed an amplifier model BLWA 0103-250 from the manufacturer BONN in Holzkirchen, Germany (Bonn Elektronik, n.d.), a class-A amplifier, which can deliver up to 250 W for an input power lower than 0 dBm. It can be controlled through an RS232 serial port, managed by the Teensy platform.

For the final prototype of the system, another type of power amplifier should be used, depending on the modulation selected. For constant envelope modulations such as frequency shift keying (FSK) and phase shift keying (PSK), a class C amplifier is the best option.

3. Tests Performed

In this section, we describe the tested combinations of power values and modulation scheme. We also detail the frame design to ensure that the channel coherence bandwidth is respected in each of the tests (Hervás et al., 2013).

Table 3
Bandwidth Transmission Tests

Order of modulation	Bandwidth transmission	Minute
2,4,8,16,32	5 KHz	05,06,07,08,09
2,4,8,16,32	10 KHz	15,16,17,18,19
2,4,8,16,32	16.66 KHz	25,26,27,28,29
2,4,8,16,32	25 KHz	35,36,37,38,39
Other tests	Other tests	45,46,47,48,49
Other tests	Other tests	55,56,57,58,59

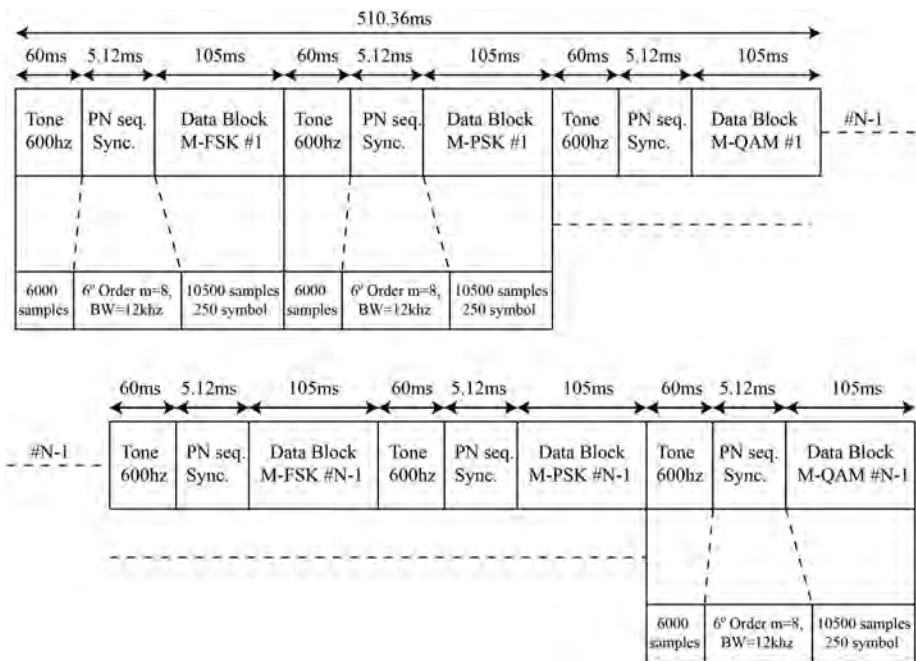


Figure 8. Frame design.

3.1. Test Bench

The entire set of tests has been classified in two groups (see Tables 2 and 3). In both groups, the PSK, quadrature amplitude modulation (QAM), and FSK modulations are tested, with a number of constellation symbols ranging from 2 to 32. In the first group, the bandwidth is fixed to 2.38 KHz, and the transmission power varies from 1 to 24 W for every modulation so the bit rate ranges from 2.38 to 11.9 kbps. In 1 hour, we perform 30 different tests as we can see in Table 2. In the second group, transmission power is fixed to 24 W, and the bandwidth varies from 2.38 to 25 KHz (see Table 3). In this case, the bit rate varies from 5 to 125 kbps.

Every group of transmissions has been working every hour for 15 days. The total amount of transmitted bits has been 16 and 20.1 MB for the first and the second groups, respectively. The second group involves more data transmitted due to the increase of bandwidth.

3.2. Frame Design

The structure of the frame is shown in Figure 8. Every test is composed by 50 packets ($N = 50$) that include three different types of modulation. Each modulation is preceded by a tone of 600 Hz and a PN sequence.

The tone is used for frequency synchronization to mitigate the effect of both the Doppler shift of the channel and the mismatch between the transmitter and receiver clocks. The PN sequence is a sixth-order m-sequence used for time synchronization, so a correlation has to be performed in real-time continuously at the receiver. The length of the frame has to be consistent with the coherence time of the channel (Proakis, 1995). Taking the most restrictive coherence time for the ordinary wave as 1.46 s (corresponding to a Doppler spread of 0.6816 Hz; Hervás et al., 2013), we set the length of the packet to 510.36 ms. In this interval, we make the test of three modulations (PSK, QAM, and FSK) with the same order of modulation, power transmission, and bandwidth. Hence, each modulation is tested under the same channels conditions.

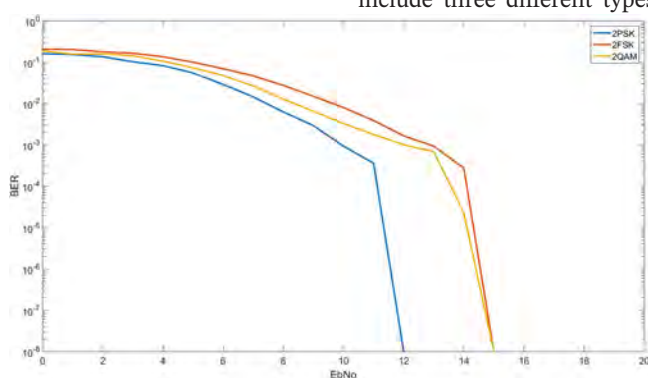


Figure 9. BER vs Eb/N_0 for second-order modulations.

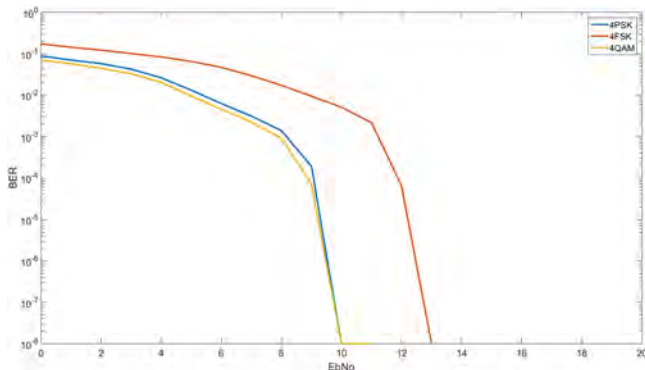


Figure 10. BER vs Eb/N0 for fourth-order modulations.

4. Results

In this section, we introduce the most relevant results of the tests performed in terms of modulation, bandwidth, and transmission power. All the data were collected during the 2018–2019 Spanish Antarctic Campaign at Livingston Island, particularly from 1 February to 2 March 2019.

4.1. Power Transmission Tests

First of all, we measured the real relationship between the bit error rate (BER) and bit energy to noise power spectral density (E_b/N_0) of the received frames. The E_b/N_0 of the signal received is calculated as:

$$(SNR) = \frac{E_b \cdot R_b}{B \cdot N_0}, \quad (1)$$

$$\frac{E_b}{N_0} = (SNR) \cdot \frac{B}{R_b}, \quad (2)$$

$$\frac{E_b}{N_0} (dB) = (SNR)(db) + 10 \cdot \log_{10}(B) - 10 \cdot \log_{10}(R_b). \quad (3)$$

The received SNR is calculated in postprocessing, R_b is the bit/rate of the signal (it must vary according to the modulation order of each test), and B is the noise bandwidth where we measure the received BER, in this case, 5 KHz (the baseband signal BW is limited to 5 KHz). Finally, the BER is calculated comparing the transmitted and received bits from a total of 25 Mb for each trace.

In Figure 9, we can see the comparison between a second-order PSK, FSK, and QAM modulations. Due to the number of transmitted bits, our system is not able to measure BER values lower than 10^{-8} . We can see that QAM and PSK are more robust than FSK because of a given E_b/N_0 . The difference between 2PSK and 2QAM is shown Figure 9. In 2PSK, both symbols are located on the real axis, while in 2QAM are located in the IQ plane. For a given bit energy, the real and complex components of the 2QAM are lower, so the performance is poorer. In order to achieve a BER of 10^{-3} , an E_b/N_0 of 10 dB is enough for 2PSK.

In Figure 10, we can see the comparison of fourth-order modulations. In this case, QAM and PSK modulations remain more robust than the FSK. 4QAM and 4PSK have exactly the same constellation so they behave in the same way. In order to achieve a BER of 10^{-3} , an E_b/N_0 of 8 dB is enough for 4PSK and 4 QAM.

For modulation orders higher than four, the received symbols are very weak for being demodulated correctly. In Figures 11 and 12, we can see the measured E_b/N_0 as a function of time of day for a transmission power of 24 W. The ionosphere reflected the signal mainly from 12:00 UTC to 19:00 UTC, so the link was available during a time window of 7 hours each day. If we look at the E_b/N_0 values, we can see values from

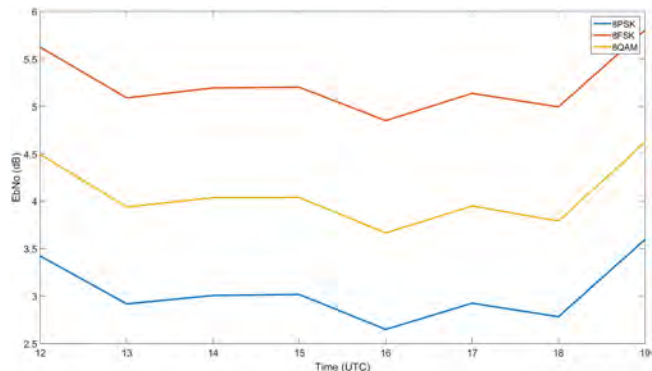


Figure 11. Eb/N0 vs time for eighth-order modulations.

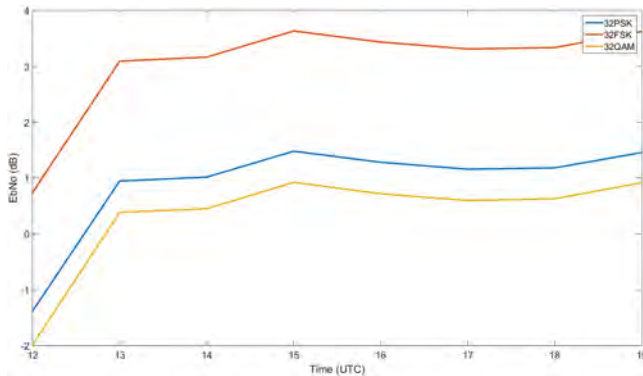


Figure 12. Eb/N0 vs time order 32 modulations.

3 to 5 dB for eighth-order modulations and from 0 to 3 dB to 32nd-order modulations. None of these values is enough to guarantee a proper demodulation of the data.

Now, we are going to study the probability to have a given BER value. For that purpose, we will make use of the cumulative distribution function (CDF) of the BER, that is, the probability of achieving a BER lower than a given value. From Figures 13–18, the axis Y shows us the probability $P(\text{BER} < X_0)$ to obtain a BER less or equal than the value X_0 of axis X. For example, the probability $P(\text{BER} < X_0)$ if $X_0 = 0.01$ is 90%, so we can assert that the 90% of the packets transmitted have a BER lower than 0.01. In Figure 13, we can see the CDF of a second-order modulation PSK, QAM, and FSK for a transmission power of 24 W. We can observe that the PSK and QAM have a probability of 95.2% and 95.4%, respectively, to achieve a BER lower than 0.004, while the probability is 92.8% for the FSK modulation.

In Figure 14, we can see the probability in case of a power transmission of 2 W. In this case, we can see that there is not a great difference between the three modulations. PSK and QAM modulations have a probability of 94.3% and 94.4% to achieve a BER lower than 0.004, respectively, in front of FSK with a probability of 93.8%.

In the case of a power transmission of 24 W for fourth-order modulations (see Figure 15), the probability for 4FSK decreases to 77.3%. The 4PSK and 4QAM have a similar behavior with a probability of 91.1% and 92.8%, respectively.

On the other hand, Figure 16 shows the CDF for a transmission power of 2 W. In this case, we can see PSK and QAM modulations still outperform FSK with a probability of 90.1% and 91.1%, respectively. For the FSK modulation the probability to have a BER lower than 0.004 decreases to 80%.

Based on the results obtained, we can conclude that a 4QAM can be used with a transmission power of 2 W, since we will have a probability about 90% to have a BER lower than 0.004. This is good enough to take into account the improvement due to the error correcting codes and the retransmissions of the frames. If we use

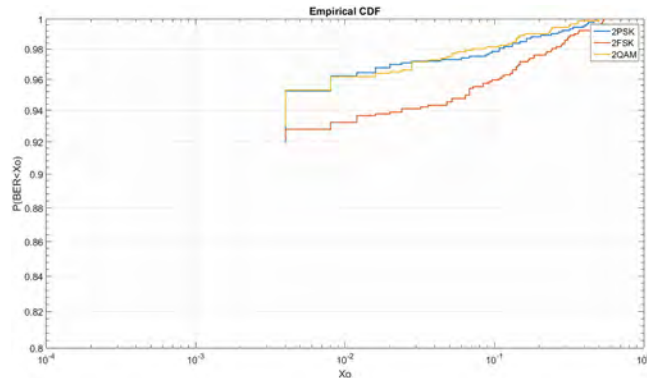


Figure 13. CDF of second-order modulations for 24 W.

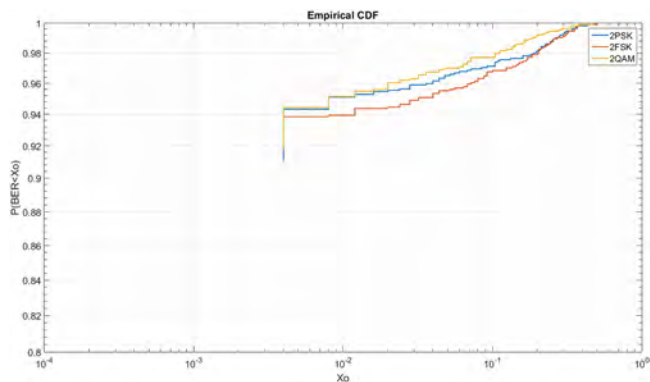


Figure 14. CDF of order two modulations for 2 W.

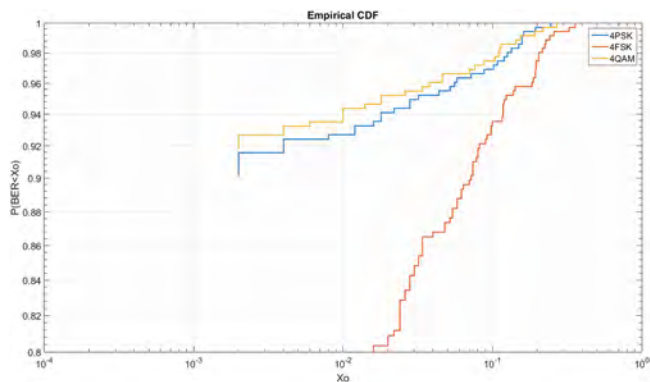


Figure 15. CDF of fourth-order modulations for 24 W.

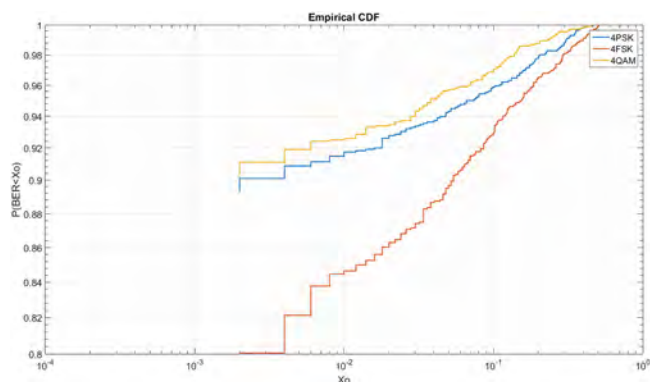


Figure 16. CDF of fourth-order modulations for 2 W.

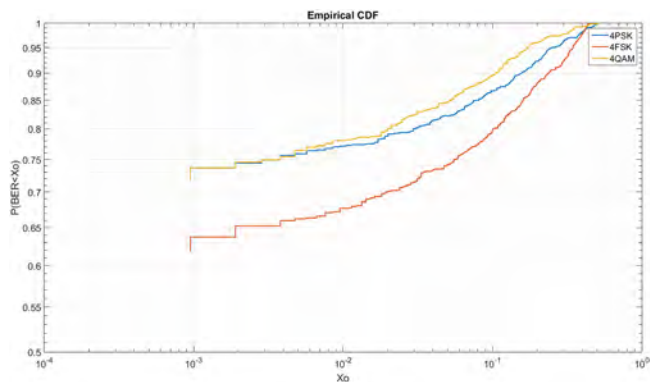


Figure 17. CDF of fourth-order modulations for BW = 5 KHz.

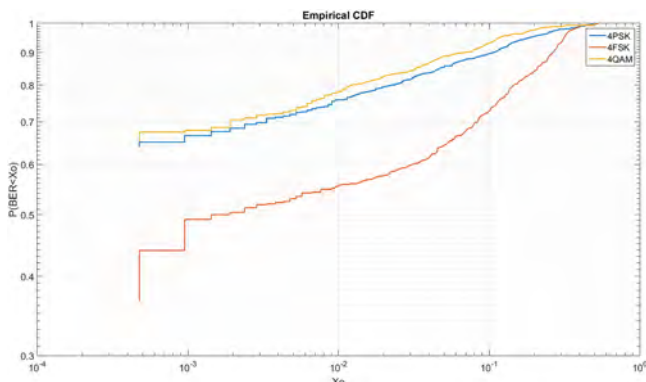


Figure 18. CDF of fourth-order modulations for BW = 10 KHz.

2PSK instead, there is a slight increase of the probability up to 94%, but the bit rate is halved. If we use a transmission power of 24 W, we could also use a simpler modulation such as 2FSK with the same performance.

4.2. Bandwidth Transmission Tests

The previous tests have been performed using a standard baseband bandwidth of 2.3 KHz. We have also tested the use of higher bandwidths out of standard. For a given modulation scheme, the bit rate is directly proportional to the bandwidth, so we can reach bit rates up to 18.4 Kbps for a 10 KHz bandwidth.

In Figure 17, we can see the CDF of the BER of fourth-order modulations for a bandwidth of 5 KHz with a transmission power of 24 W. The probability to have a BER lower than 0.001 is 73.7% for both 4PSK and 4QAM, while it is 63.8% for the FSK modulation.

The same test for a bandwidth of 10 KHz is shown in Figure 18. Here, the probability to have a BER lower than 0.001 is around 66% for both 4PSK and 4QAM, in front of 43.9% for the FSK modulation.

Although the probabilities are lower when we use higher bandwidths, we have to take into account that the bit rate is increased in a larger proportion, so the overall performance is better. If our application needs higher throughputs, we could also use greater bandwidths without increasing the power consumption.

5. Conclusions

In this paper, we have introduced a new solution for remote sensors using the NVIS communication technique. We have explored the influence of the type of modulation, the transmission power, and the bandwidth for an NVIS link between sensors located around the Spanish Antarctic Base in Livingston Island.

For low power consumption sensors, for a transmission power of 2 W, we recommend the use of the standard bandwidth of 2.3 KHz with either a 4QAM or 2PSK modulation That yields to 4.6 or 2.3 kbps with a probability around 90% to have a BER lower than 0.004 prior to any correcting code.

For sensors with higher power consumption (i.e., 24 W), we could also use the standard bandwidth with simpler modulations such as 2FSK, such a simpler amplifier could be used. If we need higher bit rates without increasing the power, we could also increase the bandwidth up to 5 KHz. In that case, we could use a 4QAM with a probability around 73.7% to have a BER lower than 0.001 for a bit rate of 9.2 kbps.

We have also defined a frame structure for NVIS communications. The frame includes a preamble for frequency and time synchronization, as well as a maximum length for each data block.

The tests prove the feasibility of NVIS for sensors located up to 250 km away from the central node, without the need of any telecom operator, and it is an interesting alternative to satellite for places without infrastructures and complicated terrain.

As we can see, the results obtained show us the specifications to achieve the robust transmission for low transmissions of sensors out of the standards. In case of an equalized 4QAM or 4PSK of 2 W and 2.4 KHz bandwidth, as we have seen, 90% of the packets transmitted have a BER lower than 0.004 in a 12.500 symbols frame and 25.000 bits. In the worst case scenarios, we will have 100 bit errors. If we apply an interleaving method and an FEC convolutional code with a rate code 1/2 as the standard MIL-STD-188-110B shows (MIL-STD-188-110B, 2000), we will improve the probability of a BER less than 0.001 to a 94%. The application of FEC will reduce the bitrate to 2.4 Kbps, this is enough for the transmission of sensor data.

The results obtained during the Antarctic campaign have been implemented for a real-time transmission of sensor data to the Spanish Antarctic Base. The implemented system did not use code correcting and interleaving methods, and a 24 W power transmission and 2.4 KHz bandwidth were used. More information about the implementation done can be found at Maso et al. (2019). In a future line of the real-time implementation of the system, a real-time ionospheric sounding, interleaving and FEC methods will be implemented in the same platform.

This work performs a study of the greatest physical layer definition for remote areas using NVIS communication. In such places, the consumption of power is one of the most critical issues in a telecommunication system design. Most of the current products in the market have a RF signal output power from 20 to 1500 W HF 3000/Thales Group, n.d.; R&S®M3SR Series4100 Software Defined Radios|System Components| Rohde & Schwarz, n.d.). In these kinds of areas, the system should be powered by batteries, which are too large. Comparing the results shown in this paper with the most commonly used internationals standards (MIL-STD-188-110B, 2000; MIL-STD-188-110D, 2017; North Atlantic Treaty Organization (NATO), 2009; STANAG 4539, n.d.), we obtain a better performance for the case of very low power consumption and without applying any interleaving method or an FEC convolutional code.

Compared to others scientific works, we can assume that the performance, in terms of BER achieved, in our system is much better than the one described in similar previous works. In the PhD thesis (Wilson, 2012), we can see a BER of 10^{-2} for an Eb/N0 of 11 dBm, with a 2-QAM and a power signal transmission of 5 W. Finally, in Saraç et al. (n.d.), we can find a real time implementation of the standard STANAG 4539 (STANAG 4539, n.d.) that achieves the minimum performance of the standard but without improving it.

Acknowledgments

This work was funded by the Ministry of Economy and Competitiveness and the European Regional Development Fund under the contract CTM2015-68902-R (MINECO/FEDE) and RTI2018-097066-B (MINECO/FEDER). The data used to develop our study and generate all the figures can be obtained online in <https://doi.org/10.5281/zendodo.3523219> and in <http://doi.org/10.5281/zendodo.3523281>.

References

- AEMET (2019). Jornada sobre las actividades de AEMET en la Antártida - State Meteorological Agency—AEMET—Spanish Government. Retrieved June 4, 2019, from http://www.aemet.es/en/noticias/2019/02/jornada_antartida
- Bonn Elektronik (n.d.). Bonn Elektronik Power amplifier 9 kHz-40GHz. Retrieved from <https://allice.de/wp-content/uploads/2017/03/Bonn-Katalog-Web.pdf>
- Davies, K. (1990). Ionospheric Radio. The Institution of Engineering and Technology, Michael Faraday House, Six Hills Way, Stevenage SG1 2AY, UK: IET. <https://doi.org/10.1049/PBEW031E>
- Hervás, M., Pijoan, J. L., Alsina-Pagès, R. M., Salvador, M., & Altadill, D. (2013). Channel sounding and polarization diversity for the NVIS channel. Proceedings Nordich HF Conference, (August).
- HF 3000/Thales Group (n.d.). Retrieved October 24, 2019, from <https://www.thalesgroup.com/en/worldwide/defence/hf-3000-skyfst>
- Ionogrames de Livingston (n.d.). Retrieved July 6, 2018, from <http://www.obsebre.url.edu/ca/ionogrames-de-livingston>
- Kodali, R. K., Boppana, L., & Kondapalli, S. R. (2013). DDC and DUC filters in SDR platforms. In *2013 15th International Conference on Advanced Computing Technologies (ICACT)* (pp. 1–6). Rajamput, India: IEEE. <https://doi.org/10.1109/ICACT.2013.6710526>
- Lauridsen, M., Nguyen, H., Vejlgaard, B., Kovacs, I. Z., Mogensen, P., & Sorensen, M. (2017). Coverage Comparison of GPRS, NB-IoT, LoRa, and SigFox in a 7800 km² Area. In *2017 IEEE 85th Vehicular Technology Conference (VTC Spring)* (pp. 1–5). Sydney, NSW, Australia: IEEE. <https://doi.org/10.1109/VTCSPRING.2017.8108182>
- LDI, Lowell Digisonde International Station List (Digisonde.com) (n.d.). Retrieved July 6, 2018, from <http://www.digisonde.com/station-list.html>
- Maso, J., Porte, J., Pijoan, J. L., & Badia, D. (2019). Internet of things communications for remote sensors in Antarctica using NVIS. In HF Nordic. Färö, Sweden.
- MIL-STD-188-110B (2000). Department of defense interface standard interoperability and performance standards for data modems.
- MIL-STD-188-110D (2017). Department of defense interface standard: Interoperability and performance standards for data modems. Retrieved from http://everyspec.com/MIL-STD/MIL-STD-0100-0299/MIL-STD-188-110D_55856/
- North Atlantic Treaty Organization (NATO) (2009). STANAG 5066: The Standard for Data Applications over HF Radio. Retrieved from <https://www.isode.com/whitepapers/stanag-5066.html>
- Porte, J., Maso, J. M., Pijoan, J. L., & Badia, D. (2019). Design, implementation, and test of an SDR for NVIS communications. *International Journal of Circuit Theory and Applications*, 47(9), 1502–1512. <https://doi.org/10.1002/cta.2670>
- Porte, J., Pijoan, J. L., Masó, J. M., Badia, D., Zaballos, A., & Alsina-Pagès, R. M. (2019). Advanced HF communications for remote sensors in Antarctica. In *Antarctica—A Key To Global Change* (1st ed.). IntechOpen.
- Proakis, J. G. (1995). *Digital communications*. New York: McGraw-Hill.
- R&S®M3SR Series4100 Software Defined Radios|System Components|Rohde & Schwarz (n.d.). Retrieved October 24, 2019, from https://www.rohde-schwarz.com/es/producto/m3srseries4100-productos-secundarios_63489-9903.html
- Red Pitaya (n.d.). Retrieved June 4, 2019, from <https://www.redpitaya.com/>
- Saraç, S., Kara, F., & Vural, C. (n.d.). Real-Time Implementation of STANAG 4539 High-Speed HF Modem. In World Academy of Science, Engineering and Technology (p. 6).
- STANAG 4539 (n.d.). North Atlantic Treaty Organization. Retrieved from <https://www.rapidm.com/standard/stanag-4539/>
- Statista - Internet of Things - Number of connected devices worldwide 2015–2025 (n.d.). Retrieved May 22, 2019, from <https://www.statista.com/statistics/471264/iot-number-of-connected-devices-worldwide/>
- Vilella, C., Miralles, D., Altadill, D., Acosta, F., Solé, J. G., Torta, J. M., & Pijoan, J. L. (2009). Vertical and oblique ionospheric soundings over a very long multihop HF radio link from polar to midlatitudes: Results and relationships. *Radio Science*, 44, RS2014. <https://doi.org/10.1029/2008RS004001>
- Wilson, J. M. (2012). A low power HF communication system. Retrieved from <https://www.escholar.manchester.ac.uk/api/datastream?publicationPid=uk-ac-man-scw:156816&datastreamId=FULL-TEXT.PDF>
- Witvliet, B. A., & Alsina-Pagès, R. M. (2017). Radio communication via Near Vertical Incidence Skywave propagation: an overview. *Telecommunication Systems*, 66(2), 295–309. <https://doi.org/10.1007/s11235-017-0287-2>
- Witvliet, B. A., van Maanen, E., Petersen, G. J., Westenberg, A. J., Bentum, M. J., Slump, C. H., & Schiphorst, R. (2015). Near Vertical Incidence Skywave Propagation: Elevation Angles and Optimum Antenna Height for Horizontal Dipole Antennas. *IEEE Antennas and Propagation Magazine*, 57(1), 129–146. <https://doi.org/10.1109/MAP.2015.2397071>